Conformational Dynamics Coupled to Protonation Equilibrium at the Cu_A Site of *Thermus thermophilus*: Insights into the Origin of Thermostability†

Nusrat J. M. Sanghamitra and Shyamalava Mazumdar*

Department of Chemical Sciences, Tata Institute of Fundamental Research, Homi Bhabha Road, Colaba, Mumbai 400005, India

Received August 31, 2007; Revised Manuscript Received December 4, 2007

ABSTRACT: An extremely slow pH dependent conformational equilibrium between a valence-delocalized and a valence-trapped species of the dinuclear Cu_A domain of cytochrome c oxidase from *Thermus thermophilus* has been identified and characterized using UV−visible absorption, circular dichroism, time-resolved fluorescence and electron paramagnetic resonance spectroscopy as well as by stopped-flow kinetic techniques. The results indicated that the nature of this pH dependent conformation change in the Cu_A domain in the *Thermus* protein was distinctly different from that observed in the mesophilic analogue from *Paracoccus denitrificans* and in the engineered Cu_A domain in azurin. pH jump kinetic studies suggested existence of a fast deprotonation equilibrium followed by slow conformational change in the protein, which is contrary to that observed in the case of the analogous protein from *P. denitrificans*. Continuous-flow electrospray mass spectral studies on H/D exchange in the $TtCu_A$ showed that ∼75% of the protons are exchanged within the dead-time of the experiment supporting fast proton transfer kinetics in the protein. Analysis of temperature dependence of the kinetics of the conformational transition showed that the rigidity of the protein structure decreases with increase in temperature. The results indicated that though the rate of proton transfer at individual sites in the protein could be very fast, the conformational change that requires simultaneous breaking of several interactions in a segment of the structure might be slow in the thermostable protein.

The extreme environmental conditions of the hyperthermal habitat have imposed the adaptive capacity in the thermophilic organisms to thrive at high temperatures where mesophilic organisms often lose their functions and nativity. Thus the proteins from thermophilic organisms, though at times very similar in structures to their mesophilic homologues, are endowed with considerably higher intrinsic resistance to thermal as well as chemical denaturation (*1*, *2*). Despite a series of intense theoretical and experimental research in this area, the molecular basis of the stability of the proteins from thermophilic organisms is not yet been unambiguously understood. Although several factors such as increased hydrophobic and electrostatic interactions, extensive H-bonds, higher compactness, enhanced polar and nonpolar contribution, enriched salt bridges, reduced ΔC_p etc. have been proposed to be responsible for the thermostability, a generalized mechanism that promotes the stability or the concept that governs this phenomenon has still remained controversial (*3*−*8*).

Both thermodynamic and kinetic factors can contribute to the thermostability of a protein. Unfolding studies of thermostable proteins have helped to gain insights into the various thermodynamic aspects of stability of these proteins (*9*−*11*). On the other hand, a handful of thermostable proteins have recently been shown to have high kinetic barriers to unfolding (*12*−*16*). Thus, the high stability of these proteins may also arise from kinetic inertness toward conformational changes in the protein scaffold (*17*). However, irreversible processes associated with the denaturation of thermostable proteins have been argued to introduce complexity in deriving the kinetic parameters associated with the unfolding of these proteins (*14*, *18*, *19*). Nevertheless, there are arguments both in favor of and against the kinetic model of thermostability of proteins (*13*−*17*, *20*−*22*). Hernandez et al. have shown by amide hydrogen exchange measurements that hyperthermophilic rubredoxin possesses conformational flexibility high enough for water and base catalyst to access the exchangeable amide with minimal structural disruption (*17*). Similarly Fitter et al. have observed an unexpectedly higher structural flexibility of thermostable α-amylase as compared to the mesophilic counterpart (*20*, *21*). These reports pose a different picture than other studies which argue that the increased conformational rigidity is the underlying phenomenon behind the enhanced thermal stability of hyperthermophilic proteins (*12*−*14*, *22*).

The unfolding and refolding can be considered as special types of conformational changes in the protein structure. It is thus necessary to probe the kinetics and thermodynamics of reversible conformational change in a thermostable protein to understand the role of local conformational dynamics in its thermostability. We have carried out a systematic study on the kinetics and thermodynamics of the pH-induced reversible conformational change in the soluble dinuclear copper protein ($TtCu_A$[1]) obtained from the solvent exposed

† The work was supported by the Tata Institute of Fundamental Research, Mumbai.

* Corresponding author. Tel: 0091 22 22782363. Fax: 0091 22 2280 4610. E-mail: shyamal@tifr.res.in. Home page: http://www.tifr.res.in/∼shyamal.

10.1021/bi701783x CCC: $40.75
Published on Web 01/12/2008

domain of the subunit II of *Thermus thermophilus* cytochrome *c* oxidase (CcO). The purple dinuclear copper center ($TtCu_A$) forms the electron entry site of the intact CcO (*23*−*26*), and although the pH-triggered conformational equilibrium between a "charge-delocalized", [$Cu^{+1.5}$−$Cu^{+1.5}$] form and a "valence-trapped" [Cu^{+1}−Cu^{+2}] form have been observed in the engineered purple Cu_A center in azurin as well as in the Cu_A center of *Paracoccus denitrificans* (*27*−*30*), such effects are yet not known in the Cu_A center from the thermostable bacteria (*31*).

Multiwavelength circular dichroism, UV−visible absorption, time-resolved fluorescence and electron paramagnetic resonance studies on pH dependence of $TtCu_A$ enabled us to identify an extremely slow pH-induced conformational change in the thermostable protein, which was distinctly different from their mesophilic analogues. Kinetics of this conformational transition has been studied at different temperatures and pH to determine the activation parameters as well as the mechanism of the process. Continuous-flow electrospray mass spectral studies on H/D exchange were carried out to understand the kinetics of proton transfer in the protein. The results have been discussed in the light of understanding the origin of thermostability of the protein.

MATERIALS AND METHODS

Protein Purification. The soluble fragment of subunit II of CcO of *T. thermophilus* was expressed and purified according to the procedure reported by Slutter et al. (*32*). The gene of $TtCu_A$ was inserted to *Nco*I and *Bam*HI restriction sites. The plasmid pMA10 was transformed into *Escherichia coli* BL21 strain. The SDS PAGE of the purified Cu_A showed a single band corresponding to 99% purity. For the pure holoprotein the ratio of the absorbance at 276 and 530 nm was found to be 6.7, which agreed with an earlier report (*32*). Protein concentration was measured using an extinction coefficient (ϵ_{480}) of 3.1 mM^{-1} cm^{-1} at 480 nm (*32*). All chemicals used were of the highest analytical grade.

Spectroscopic Methods. The pH-induced conformational changes of $TtCu_A$ were monitored by UV−visible absorption, circular dichroism in the far-UV, near-UV and visible regions, EPR and fluorescence spectroscopic techniques. The pH was varied from 6.5 to 12 using the universal buffer (mixture of 0.2 M boric acid, 0.05 M citric acid and 0.1 M trisodium orthophosphate·$12H_2O$; pH was adjusted with 0.1 M NaOH) and the solutions were equilibrated at each pH for 48 h at each temperature under nitrogen atomosphere for spectroscopic studies at that temperature. The reversibility of the conformational transition was checked by varying the pH in both directions. pH of the protein solution was corrected at each temperature for temperature dependent kinetic as well as equilibrium studies.

Circular dichroism studies were carried out using a Jasco J-810 spectropolarimeter. Near-UV and visible CD experiments were carried out using a protein concentration of 50 μM and a cuvette of 10 mm path length in the spectral ranges of 250−350 and 300−700 nm, respectively. Far-UV CD spectra were measured over the 180−260 nm range in a cuvette of 1 mm path length using protein concentration of 5 μM. A good signal-to-noise ratio in the CD spectra was obtained on data averaging over three scans.

The absorbance as well as the CD data in the visible region obtained from the pH titration experiment were fitted to the one-site protonation/deprotonation equilibrium model. A global fit was carried out for the data points at multiple wavelengths using eq 1,

$$A^{\lambda}_{obs} = \frac{C_0\{\epsilon^{\lambda}_A + (\epsilon^{\lambda}_B \times 10^{pH-pK_a^{app}})\}}{1 + 10^{pH-pK_a^{app}}} \quad (1)$$

where the observed absorbance (A^{λ}_{obs}) at wavelength λ was related to the molar extinction coefficients or CD values (ϵ^{λ}_A and ϵ^{λ}_B) for the species A ("low-pH" form) and species B ("high-pH" form) that are in equilibrium (A ⇌ B) at a given pH.

Kinetic studies were carried out using a Perkin-Elmer Lamda 25 UV/vis spectrometer as well as using a HiTech SF61MX stopped-flow spectrometer. Protein solution was prepared in universal buffer of pH range 6.5 to 12 stated above. The absorbance change at 530 nm with respect to time was monitored at different pH and different temperature.

The EPR measurements were carried out at 9.42 GHz (X band) with a Bruker 200D spectrometer equipped with an Oxford Instruments continuous-flow helium cryostat (ESR 900) with a temperature accuracy of ±1 K.

All the steady-state fluorescence measurements on the $TtCu_A$ at different pH were carried out using a SPEX fluorolog (T-format) FL111 spectrofluorimeter by exciting Trp64 at 295 nm. Time-resolved fluorescence intensity decay measurements were carried out using a time-correlated single photon counting (TCSPC) setup, and 1 ps pulses of 887 nm radiation from the Ti-sapphire femto/picosecond (Spectra Physics, Mountain View, CA) laser, pumped by an Nd:YLF laser (Millenia X, Spectra Physics), were frequency tripled to 295 nm by using a frequency tripler (GWU, Spectra physics) for exciting the tryptophan residue in the protein. Fluorescence decay curves were obtained at the laser repetition rate of 4 MHz by a micro-channel plate photomultiplier (model R2809u; Hamamatsu Corp.) coupled to the TCSPC setup. The instrument response functions (IRF) at 295 nm were obtained using a dilute colloidal suspension of dried nondairy coffee whitener. The width (fwhm) of the IRF was 40 ps. Fluorescence emission measurements from protein samples, excited at 295 nm, were monitored at 330 nm at the magic angle (54.7°) by using a combination of a monochromator and a 320 nm cutoff filter. The fluorescence decay curves at the magic angle were analyzed by deconvoluting the observed decay with the IRF to obtain the intensity decay function represented as a sum of two, three or four exponentials:

$$I(t) = \sum_i \alpha_i \, e^{-t/\tau_i} \qquad i = 2-4 \quad (2)$$

[1] Abbreviations: CcO, cytochrome c oxidase; $TtCu_A$, the soluble dinuclear copper protein from the solvent exposed domain of the subunit II of *Thermus thermophilus* CcO; TCSPC, time-correlated single photon counting; CD, circular dichroism spectrometry; ESI MS, electrospray ionization mass spectrometry; P_AH, protonated form of "low-pH" conformation of the Cu_A site; P_BH, protonated form of "high-pH" conformation of the Cu_A site; P_A^-, deprotonated form of "low-pH" conformation of the Cu_A site; P_B^-, deprotonated form of "high-pH" conformation of the Cu_A site.

where $I(t)$ is the fluorescence intensity at time t and α_i is the amplitude of the ith lifetime τ_i such that $\sum_i \alpha_i = 1$.

Electrospray mass spectra were obtained using a Thermo Finnigan LCQ Deca Electrospray quadrupole ion trap mass spectrometer. Capillary temperature was maintained at ~100 °C, and the capillary voltage was kept at 31 V. The ion-spray voltage was maintained at 4.5 kV, and the ion optics was tuned to get the maximum ion count. The protein solutions (2 μM) for H/D exchange studies were prepared in Milli Q water, and mixing of D_2O was done in a continuous-flow setup to minimize the dead time of the H/D exchange. The data was collected over 10 s, and maximum dead time of H/D exchange estimated from the mixing time, flow rate of the sample injection and the data collection time was ~30 s.

RESULTS AND DISCUSSION

Existence of a Conformational Switch between Low-pH and High-pH Forms. $TtCu_A$ is a purple colored protein having characteristic absorption bands in the visible region at 365, 477, 530, 790 nm (*32*). No change was observed in the absorption spectra of the protein even after 24 h, when the pH of the sample was decreased to 3.5. Moreover, we have recently shown that holoprotein both in the native mixed-valence state and in the reduced state of the metal ions and the apoprotein of $TtCu_A$ were extremely stable both toward thermal unfolding and guanidine hydrochloride induced unfolding at pH 7 (*33*).

Increase in pH also did not immediately show any change of the spectra of the protein solution unlike in case of the *Paracoccus* Cu_A reported earlier (*27*). However, increase in pH of the $TtCu_A$ solution was found to cause a slow but distinct change in the spectra indicating changes in the environment around the metal ion at high pH. The spectral change on increase in pH was markedly slow and the intensities of all the visible absorption bands were decreased with consecutive increase in intensity at ~320 nm with an isosbestic point at ~355 nm (Figure 1A) with increase in pH. The protein solution was incubated for 48 h under nitrogen atmosphere at each pH ranging from 6.5 to 12 to ensure equilibrium at each pH. The nature of the buffer (universal buffer) did not have any effect on the spectrum of the protein other than changing pH of the medium.

Analogous observation of pH dependence in the visible CD spectra of the protein, where the intensities of CD bands at 521 nm and 468 nm were decreased with increase in pH (Figure 1B), supports the possibility of conformational change at the dinuclear Cu_A site at higher pH. The CD spectrum of the protein in the far-UV region (190−260 nm) did not change significantly upon increase in pH from 6.5 to 12 (Figure S1, Supporting Information). Unfortunately, the far-UV CD data at wavelengths <190 nm was not reliable at high pH due to buffer absorption. Nevertheless, absence of changes in the far-UV CD spectrum of $TtCu_A$ in the 190−260 nm range was corroborated by quantification of the secondary structure using Jasco Secondary Structure Estimation Program (*34*), which indicated almost no change in the secondary structure (45% β sheets and 2% α helix) of the protein. However, the CD spectrum of the protein in the near-UV and visible region (>260 nm) was drastically changed on transition from "low-pH" to the "high-pH" forms (Figure 1B) indicating change in the tertiary structure of the protein.

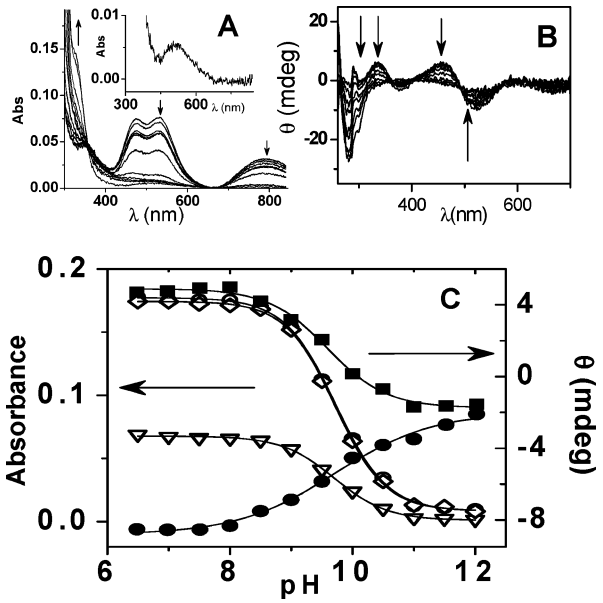

FIGURE 1: (A) Variation of the UV−visible absorption spectra of $TtCu_A$ (12 μM) with increasing pH from 6.5 to 12. (Inset shows the 512 nm band of $TtCu_A$ at pH 12.) (B) Variation of visible CD spectra of $TtCu_A$ (50 μM) with increasing pH from 6.5 to 12. (C) The variation of absorbance of $TtCu_A$ (30 μM) with pH: ▽ at 790 nm; ◇ at 477 nm; ○ at 530 nm) (left layer). The variation of CD of $TtCu_A$ (50 μM) with pH: ■ at 468 nm; ● at 521 nm) (right layer). Solid lines represent fit to the data points using eq 1.

Figure 1C shows the variation in the absorbance and CD at different wavelengths as a function of pH that could be analyzed by a one-site protonation/deprotonation equilibrium model (eq 1). An apparent pK_a value of pK_a^{app} =9.7 was obtained for this equilibrium at 25 °C. The pH-induced conformational transition was reversible in nature as observed in the restoration of 92% of the original spectrum of the protein upon decreasing the pH from 12 to 6.5 on incubation for ~48 h. This supported that there was no release of free copper ion from the protein on increasing pH, which agreed with earlier reports on the mesophilic Cu_A protein (*27*). Lappalainen et al. showed that at pH 7.0, the Cu_A from *Paracoccus denitrificans* (*Paracoccus* Cu_A) shows absorption bands at 360, 480, 535 and 810 nm, which are similar to those of the $TtCu_A$ (*30*). We have earlier shown (*27*) that an increase in pH from 6.5 to 10 causes a pH-induced conformational change in the *Paracoccus* Cu_A analogous to that observed in the present case for the $TtCu_A$. However, the pK_a^{app} for this transition in the *Paracoccus* Cu_A protein was 8.2 at room temperature, which is much lower than that observed in the present case (pK_a^{app} = 9.7). Comparison of the spectral features of $TtCu_A$ with those of *Paracoccus* Cu_A shows that the "high-pH" form of Cu_A obtained from both these sources has reduced intensity of visible absorption bands, but the near UV absorption spectra of the Cu_A centers of $TtCu_A$ were markedly different from those of *Paracoccus* Cu_A at high pH. The *Paracoccus* Cu_A shows an increase in the intensity of the 360 nm peak with increase in pH, which was otherwise of less intensity at ambient pH, whereas in the case of $TtCu_A$, there appeared a new band at 320 nm along with the decrease in the intensity of 365 nm peak with increase in pH and at pH 12 another band at 512 nm (Figure 1A and the inset).

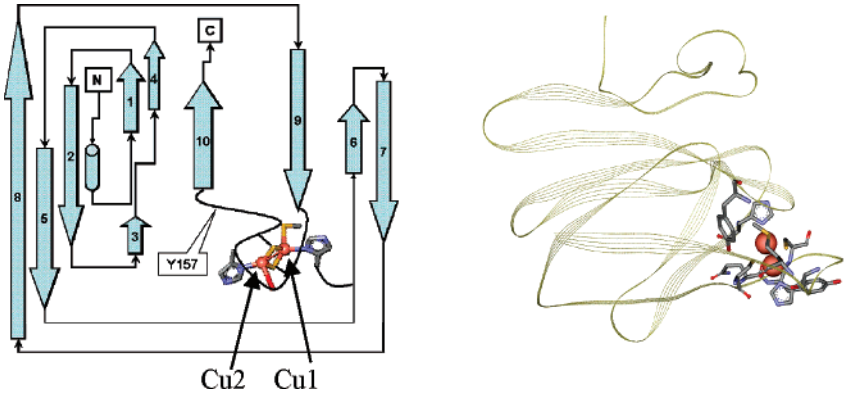

FIGURE 2: Schematic wire diagram and structure of the soluble Cu_A domain of subunit II of cytochrome c oxidase from *Thermus thermophilus*. The coordinates are taken from the RCSB Protein Data Bank, http://www.rcsb.org/pdb/home/home.do (PDB code: 2CuA.pdb).

The reported crystal structure of the $TtCu_A$ (PDB code 2CUA.pdb, Figure 2) corresponds to the "low-pH" form that is present at ambient pH (*35*). The crystal structure shows that this protein has a β barrel structure (*35*, *36*) in which two Cu atoms (Cu1 and Cu2) in the Cu_A center are strongly coordinated to His114, Cys149, Cys153, His157 and weakly coordinated to Gln151 and Met160. The two cysteine residues (Cys149 and Cys153) bridge the two Cu atoms and form a dimeric Cu_2S_2 structure. The absorption bands at 477 nm, 530 nm of the Cu_A center have been assigned to extensive S(Cys)→Cu charge transfer (CT) transitions in the rhombic Cu_2S_2 dimeric core, and the 790 nm band was assigned to the transition associated with the valance-delocalized Cu_A center (*37*). Similarly the 365 nm band was attributed to the (His)N→Cu interactions (*37*). pH-induced conformational change indicated by the reduced intensities of the visible absorption bands in the case of *Paracoccus* Cu_A was ascribed to a distortion in the coordination site of the dicopper center (*27*). Along with the striking reduction in the intensity of the visible absorption bands, the evolution of new spectral features (intense peak at 320 nm and a weak band at 512 nm) at higher pH in $TtCu_A$ enunciates a possibility of significant alteration and distortion in the coordination environment of the dinuclear copper center. Since the origin of the visible absorption bands at 477 and 530 are the S(Cys)→Cu CT transitions, the depletion of these bands indicates the weakening or absence of these transitions, suggesting the collapse of the doubly bridged Cu_2S_2 core (*37*). Thus the rhombic Cu_2S_2 core of the $TtCu_A$ may be disrupted at high pH and the nature of the (His)N→Cu CT transition is also likely to have changed. These results indicate that the native "charge-delocalized" [$Cu1^{1.5+}$—$Cu2^{1.5+}$] form of the metal center that is present at ambient pH is converted into a "valence-trapped" form with either [$Cu1^{2+}$, $Cu2^{1+}$] or [$Cu1^{1+}$, $Cu2^{2+}$] species at high pH. The crystal structure (*35*) of $TtCu_A$ shows that the two copper centers are not equivalent and the bridging cysteines are closer to Cu2 that is coordinated to His157 and Gln151. However, the observed spectroscopic changes may result from several possibilities. The formation of the high-pH form may involve breaking of the dithiolate bridges resulting in the cysteines bound to the reduced $Cu2^{1+}$ center in a [$Cu1^{2+}$, $Cu2^{1+}$] configuration, which could result in disappearance of the S(Cys)→Cu CT transitions in the visible spectrum at high pH. The observation of an intense band at 320 nm at high pH may also arise from a strong S(Cys)→Cu CT transition in a tetragonal copper center as observed in chimeric Cu proteins (*38*). Mixed ligand model copper complexes (*39*) were earlier shown to give $\sigma(S)-d_{x^2-y^2}(Cu^{2+})$ CT transitions at 333 nm, which supports this possibility. However, a pH-induced conformation change leading to strengthening of the Cu1−His114 bond that was longer (2.11 Å) compared to the Cu2−His157 bond (1.88 Å) in the "low-pH" form giving rise to an increased intensity of the 320 nm band in the "high-pH" form also cannot be ruled out.

Analogous to the earlier results (*31*), the $TtCu_A$ was found to be extremely thermostable in the pH range of the present study. There was practically no unfolding of the protein observed up to 95 °C at all pH from pH 6 to pH 12. In order to determine the thermodynamic parameters associated with the pH-induced conformational change in the $TtCu_A$, we determined the pK_a^{app} for the "low-pH" form ⇌ "high-pH" form equilibrium at different temperatures. The pH values were adjusted at each temperature to avoid error due to temperature dependence of the buffer capacity. The results show that the pK_a^{app} decreased linearly with increase in temperature (see Figure S2, Suppporting Information). The results were analyzed using the van't Hoff equation, and the value of the associated enthalpy change (ΔH_a^{app}) was found to be 123 (±5) kJ/mol and the corresponding entropy change (ΔS_a^{app}) was 234 (±20) J/mol/K.

The absorption and CD spectral data suggest a conformational transition from a "low-pH" form to a "high-pH" form of the $TtCu_A$, and the nature of this conformational change is distinctly different from that observed in the *Paracoccus* Cu_A (*27*).

pH Dependence of the Time-Resolved Fluorescence of $TtCu_A$. In order to understand the nature of the conformation change associated with the conversion of the "low-pH" form to the "high-pH" form, we carried out steady-state and time-resolved tryptophan fluorescence studies of the protein at different pH.

$TtCu_A$ consists of a single trytophan residue (Trp 64), which can serve as a probe for conformational changes in the protein. The fluorescence quantum yield as well as the life time of the time-resolved fluorescence decay of the tryptophan residue would be affected due to quenching by the metal center, and any change in the conformation at the metal center or near the tryptophan residue would change the quenching efficiency (*40*). The intensity of the tryptophan emission band (λ_{ex} = 295 nm, λ_{em}(max) = 325 nm) was

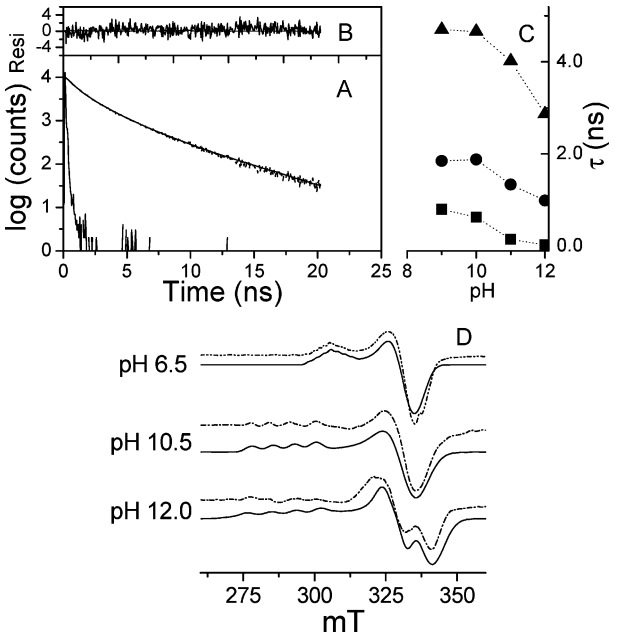

FIGURE 3: (A) Time-correlated single photon counting data for Trp fluorescence ($\lambda_{ex} = 295$ nm and $\lambda_{em} = 330$ nm) of $TtCu_A$ (50 μM) at pH 12 along with the instrument response profile; the solid line passing through the data points represents a three exponential fit (eq 2); (B) plot of the weighted residuals; (C) variation of the life times (τ_1 (square), τ_2 (circle) and τ_3 (triangle)) obtained from the discrete exponentials analysis of tryptophan fluorescence of $TtCu_A$ (50 μM) with pH; (D) X-band ESR spectra of $TtCu_A$ (1 mM) at different pH. Experimental conditions: temperature 4 K, microwave frequency 9.42 GHz, microwave power 10 dB. Dashed lines are experimental spectra, and solid lines correspond to simulated spectra.

found to decrease with increase in pH of the protein solution. The emission band was found to become slightly broad at high pH, indicating possible increase in polarity of the environment around the tryptophan residue at high pH (see Figure S3, Supporting Information). The decrease in Trp fluorescence intensity at high pH could be due to the decrease in distance or change in the relative orientation between Trp residue and copper center (*41*). The Trp fluorescence lifetime decay profiles (Figure 3A) for the $TtCu_A$ obtained by the time correlated single photo counting technique could be fitted to a triple exponential decay function using the discrete exponentials model (eq 2, $i = 3$) at each pH. The amplitude parameters associated with each lifetime component were found to remain almost unchanged over the whole pH range studied (see Table S1, Supporting Information). The goodness of fit was ascertained from the chi-square ($\chi^2 \sim 1$) and from the randomness of the residuals distribution (Figure 3B). All the three lifetime components (τ_1, τ_2 and τ_3) decreased with increase in pH (Figure 3C). The discrete analysis of the fluorescence decay (eq 2) for a heterogeneous solution containing both the "low-pH" and "high-pH" forms of the protein would give a weighted average of the lifetime values at each pH. This decrease in the lifetime thus could be due to the decrease in the distance of the tryptophan residue (Trp 64) from the copper centers (Cu_A) due to the conformational change occurring during the conversion of "low-pH" form to "high-pH" form. This further confirmed that there is indeed a conformational change in the protein on increase in pH and this change in the tertiary structure possibly involves movement of the strand-1 toward the strand-9 due to distortion in the β-barrel of the protein (Figure 2) bringing the Trp64 closer to the metal centers.

EPR Spectra of $TtCu_A$ at Different pH. To obtain further insight into the oxidation state and coordination geometry of the metal ion in the "low-pH" and "high-pH" forms of the protein, EPR spectra at various pH were recorded at 4 K. Figure 3D shows the X-band EPR spectra of $TtCu_A$ at 4 K at ambient pH (6.5) and at higher pH (10.5 and 12). At ambient pH (pH 6.5), the EPR spectrum of $TtCu_A$ showed an axial signal, $g_\perp \sim 2.00$ and $g_{||} \sim 2.18$ as reported earlier (*32*, *42*, *43*). The typical splitting of the $g_{||}$ indicative of delocalization of one unpaired electron over two equivalent copper atoms (class III) could not be resolved in the present case, suggesting that the hyperfine coupling constant is very small ($A_{||} \sim 2.5$ mT), which agrees with earlier reports on the $TtCu_A$ (*32*) as well as on other chimeric Cu_A proteins (*28*, *44*). As pH was increased from 6.5 to 10.5, the EPR signal in the $g_{||}$ region changed significantly with increased copper hyperfine splitting signals. Simulation of the EPR spectrum at pH 10.5 (Figure 3D) gave the values of $g_x \sim 2.00$, $g_y \sim 2.01$ and $g_z \sim 2.30$, with $A_x \sim A_y = 2.5$ mT and $A_z = 7.5$ mT, which are similar to those of the "high-pH" form of the *Paracoccus* Cu_A consistent with a "valance-trapped" [Cu^{2+}, Cu^{1+}] configuration reported earlier (*30*). The EPR spectrum of the protein at pH 12 was found to be very broad and indicated the presence of a mixture of at least two isolated Cu^{2+} species with A_z values 10 mT and 8.5 mT (Figure 3D). The presence of four lines in the EPR spectra of $TtCu_A$ at pH 12 is indicative of a "valence-trapped" species where a single copper nucleus is coupling to the unpaired electron and the species may not be totally homogeneous. Similar pH dependent changes in the EPR spectra were observed by Farrar et al. in the case of *Paracoccus* Cu_A protein at pH 10 and in the H252N mutant of the same protein (*29*). Thus the EPR spectra of the $TtCu_A$ protein at different pH in the present case indeed suggest that the metal center has been converted from the native "charge-delocalized" form to "valence-trapped" [Cu^{+2}, Cu^{+1}] (*28*, *29*) form(s) at high pH.

The EPR along with the fluorescence and absorption spectral results suggest that increase in pH not only leads to the breaking of the "charge-delocalized" dinuclear copper center in the $TtCu_A$ but also causes drastic change in the tertiary organization of the strands in the protein. The pK_a of this change ($pK_a^{app} = 9.7$) is close to the pK_a for deprotonation of the OH− of a tyrosine or of the NH− of a histidine or of the SH− of a cysteine or of the NH_3^+ of a lysine residue. The last two possibilities can be ruled out as both the cysteines present in the $TtCu_A$ exist as deprotonated forms to coordinate to the copper centers, and all the lysine residues in the protein are solvent exposed and too far away from the metal centers to cause any change in the geometry of the metal site on deprotonation. The change in the conformation at the metal binding site is possibly initiated by deprotonation of a tyrosine or a histidine residue in the protein. The pK_a of the NH− proton of histidine varies over a large range depending upon the environment and presence of prosthetic group in the protein (*45*). The N^{δ}− of His114 is coordinated to Cu1, and the pK_a of the imidazole is known to change drastically upon complexation with a metal ion (imidazole pK_a = 14, metmyoglobin imidazole pK_a ~10)

(*46*, *47*). Deprotonation of the $N^{\epsilon}H-$ of His114 could also enhance the electron density at the $N^{\delta}-$ of the imidazole ring strengthening the $Cu1^{2+}-$His114 bond at high pH, which is one of the possibilities that could give rise to the new absorption band at 320 nm in the "high-pH" form of the protein (Figure 1A). The $N^{\epsilon}-$ of His114 is hydrogen bonded to Asp111 in the protein at pH 7.0, thus the observed pK_a (9.7) in the present case could correspond to deprotonation of the $N^{\epsilon}H-$ of the coordinated histidine residue in the protein in the "valence-trapped" form. Deprotonation of the His157 that is coordinated to Cu2 could have slightly higher pK_a. The mixture of species observed in the EPR spectrum of the protein at pH 12 might arise due to the presence of another configuration of the "valence-trapped" form in the solution at high pH. Apart from the coordinated histidines, deprotonation of tyrosines could also result in the conformational change in the metal center of the protein. The $TtCu_A$ protein consists of 7 Tyr residues (*32*) of which two (Tyr90 and Tyr157) are located close to the metal centers. Tyr90 resides on the 3rd strand at ~5 Å away from the Cu_A site while Tyr157 is on the loop connecting 9th and 10th strands of the β-barrel. The crystal structure (PDB code: 2CuA.PDB, Figure 2) further indicates that Tyr90 is hydrogen bonded to Gly115 connecting strand 3 to 6. Deprotonantion of the Tyr90 could cause a distortion at the cupredoxin fold leading to a conformation change at the metal center. It is however important to note that the exact nature of the pH-induced conformation change cannot be specified from the present results.

Mechanism of the pH-Induced Conformational Change. The conversion of the "low-pH" form to the "high-pH" form could involve a deprotonation step followed by a conformational rearrangement step. In the initial step, an amino acid (could be a histidine or a tyrosine residue) is deprotonated, which leads to the formation of a deprotonated species without affecting the conformation. A conformational rearrangement step might follow this deprotonation step in which subtle changes in the tertiary structure around the metal takes place leading to the formation of the "high-pH" form. In order to gain insight into the mechanism of conversion of the "low-pH" to the "high-pH" form, the kinetics of the process was studied by monitoring the absorbance at 530 nm at different pH. Unlike in the case of the *Paracoccus* protein (*27*), the pH-induced conformational change in the $TtCu_A$ was found to be extremely slow. The thermostable protein takes almost 48 h to equilibrate at each pH whereas in the mesophilic counterpart the whole process occurs on the millisecond time scale (*27*).

The rate of change in the absorbance of the protein at 530 nm followed by a pH jump was measured at different final pH (pH_f) from the same initial pH ($pH_i = 6.5$). The rate of the reaction was found to be slow in the low pH range where the kinetics was monitored with the spectrophotometer, while the rate was relatively faster in the higher pH range ($pH_f > 11.5$) and kinetics was monitored using the stopped-flow spectrometer in the higher pH range. The time evolution of the observable (A_{530}) subsequent to a pH jump could be fitted to single-exponential decay function, and apparent rate constant k_{app} was determined (Figure 4A and B) at each pH (pH_f). Our earlier studies on the *Paracoccus* protein showed that there could be two possible models for the pH-induced conversion (*27*). The first model consists of a slow (rate

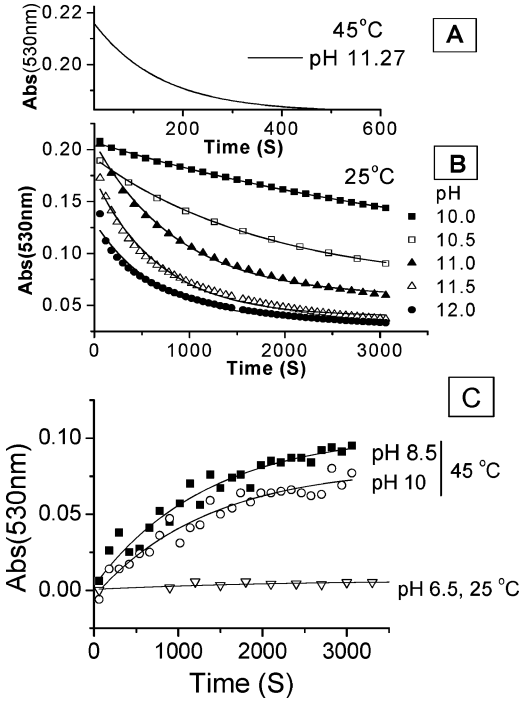

FIGURE 4: (A) Representative stopped-flow profile showing time dependent variation of absorbance of $TtCu_A$ (35 μM) at 530 nm (pH 11.27, temperature 45 °C). (B) Time dependent variation of the absorbance of "low-pH" form of $TtCu_A$ (35 μM) at 530 nm subsequent to a pH jump from pH 6.5 to pH 10, ■; to pH 10.5, □; to pH 11.0, ▲; to pH 11.5, △; and to pH 12.0, ●. The solid lines through the data points are the single-exponential fits. (C) Time dependent variation of the absorbance of "high-pH" form of $TtCu_A$ (20 μM) at 530 nm subsequent to a pH jump from pH 12 to pH 8.5, ■; to pH 10, ○ at 45 °C; and to pH 6.5, ▽ at 25 °C.

determining) proton transfer step (step 1) followed by a fast (equilibrium) conformation change (step 2). The apparent rate constant (k_{app}) in this model (*27*) would linearly increase with proton concentration ($[H^+]_f$). The second model consists of a fast equilibrium in step 1 (proton transfer), which is followed by a slow conformational change in step 2 as shown in Scheme 1. The apparent rate constant (k_{app}) in this model would increase with decrease in the proton concentration.

Scheme 1

$$\text{step 1:}\quad \text{low-pH form } (P_AH) \underset{K_a}{\rightleftharpoons} \text{low-pH form } (P_A^-) + H^+ \qquad (3)$$

$$\text{step 2:}\quad \text{low-pH form } (P_A^-) \underset{k_2}{\overset{k_1}{\rightleftharpoons}} \text{high-pH form } (P_B^-) \qquad (4)$$

$$k_{app} = k_2 + \frac{K_a k_1}{K_a + [H^+]} \quad \text{and} \quad K_a^{app} = K_a \frac{k_1}{k_2} \qquad (5)$$

In Scheme 1, K_a is the proton transfer equilibrium constant; k_1 and k_2 are the forward and backward rate constants for the conformation change respectively.

The magnitude of k_{app} in the present case of $TtCu_A$ was found to increase with the increase in the value of the final pH (pH_f) in the pH jump experiment (see Figure 5A) and followed the model (eqs 3 and 4) described above. Analyses of the results showed that the values of the rate constants (k_1 and k_2) associated with the conformation change in the protein are very small ($k_1 = 0.002\ s^{-1}$, $k_2 = 1.3 \times 10^{-4}\ s^{-1}$ at 25 °C) and the value of the K_a for the deprotonation (step 1, eq 3) equilibrium determined from the pK_a^{app} (eq 5)

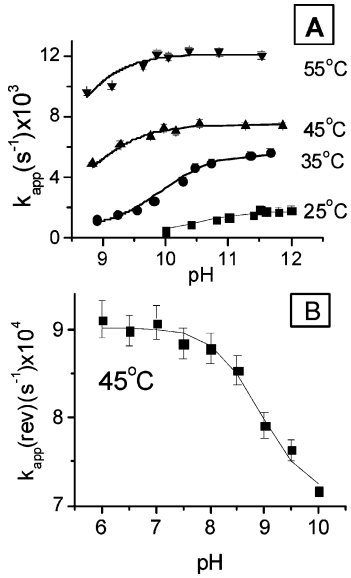

FIGURE 5: (A) Variation of k_{app} of pH-induced conformational change of "low-pH" form of $TtCu_A$ with pH at different temperatures: ■ at 25 °C; ● at 35 °C; ▲ at 45 °C; ▼ at 55 °C. (B) Variation of k_{app} of pH-induced conformational change of "high-pH" form of $TtCu_A$ with pH at 45 °C ■; vertical lines represent experimental errors.

obtained from the equilibrium experiment was found to be $K_a = 4.06 \times 10^{-11}$ M^{-1} ($pK_a = 10.4$) at room temperature. These results suggest that the conformational change in the protein subsequent to the deprotonation of the residue (with $pK_a = 10.4$) occurs quite slowly. Earlier studies showed that the mesophilic Cu_A protein undergoes a fast conformation change following a slow deprotonation step (*27*).

The reverse conversion of the "high-pH" form to the "low-pH" form by decreasing the pH of the "high-pH" species was found to be much slower (Figure 4C) compared to the forward reaction (Scheme 1). Moreover, unlike in the case of the forward reaction (Scheme 1), the rate of the reverse reaction was increased with decrease in the final pH (pH_f) of the solution, indicating that the mechanism of the reverse reaction possibly follows the scheme (Scheme 2) consisting of a fast protonation (step 3) followed by a slow conformation change (step 4) of the protonated species.

Scheme 2

$$\text{step 3:}\quad \text{high-pH form } (P_B^-) + H^+ \underset{K_a^r}{\rightleftharpoons} \text{high-pH form } (P_BH) \qquad (6)$$

$$\text{step 4:}\quad \text{high-pH form } (P_BH) \underset{k_3}{\overset{k_4}{\rightleftharpoons}} \text{low-pH form } (P_AH) \qquad (7)$$

$$k_{app}^r = k_3 + \frac{k_4[H^+]}{K_a^r + [H^+]} \qquad (8)$$

In Scheme 2, K_a^r is the associated proton transfer equilibrium constant for protonation of the "high-pH" form (P_B^-) prior to the conformation change to the "low-pH" form (P_AH); k_4 and k_3 are respectively the forward and backward rate constants for the formation of the native "low-pH" conformation from the protonated state (P_BH) of the "high-pH" conformation.

The apparent rate constant for the reverse reaction, k_{app}^r, was found to be extremely small ($\sim 5 \times 10^{-4}$ s^{-1} at 25 °C for $pH_f = 6.5$), and it decreased with increase in the value of the final pH (pH_f) in the pH jump experiment. Figure 5B shows typical variation of k_{app}^r with pH at 45 °C. The error in estimating k_{app}^r was significantly large because of the extremely slow kinetics; reliable values could only be obtained at different pH (in the range from pH_f 10 to 6.0) at 45 °C, and the data could be fitted to the model shown in Scheme 2 (eq 8).

Analyses of the results showed that the values of the rate constants (k_3 and k_4) associated with the conformation change in the protein in the protonated form are about 10-fold smaller ($k_3 \sim 0.007$ s^{-1}, $k_4 \sim 2 \times 10^{-4}$ s^{-1} at 45 °C) than the corresponding rate constants (k_1 and k_2) in Scheme 1 at the same temperature. The value of the equilibrium constant, K_a^r (1.1×10^{-9} M^{-1}), for the deprotonation in Scheme 2 (step 3, eq 6) was found to be comparable to the K_a (1.3×10^{-9} M^{-1}) in Scheme 1 (step 1, eq 3) at 45 °C. These results suggest that the conformational change in the protein subsequent to the deprotonation/protonation of a residue (could be a coordinated histidine or a tyrosine residue) occurs quite slowly. Moreover, the conformation dynamics in the protein was relatively faster when the residue is deprotonated (P_A^- and P_B^-) compared to that when it is protonated (P_AH and P_BH). Nevertheless, the rate of the conformation change is much slower than the protonation/deprotonation of the protein in both cases. It is important to note that the present results indicate that there is possibly no change in the spectra of the metal center subsequent to the deprotonation/protonation step (step 1 or step 3), and spectral change takes place only on conformational change at the metal center.

These results suggest that the $TtCu_A$ not only has possession of exceptional thermodynamic stability (*31*) but also is kinetically very inert. The slow conformational change observed in the present case agrees with earlier reports on slow conformational changes in several other thermostable proteins (*12*−*16*). However, earlier studies (*17*) on deuterium exchange kinetics by NMR (*17*) showed that the amide H/D exchange rates for different residues in the thermostable rubredoxin from *Pyrococcus furiosus* are very fast, suggesting high flexibility of the protein backbone. The conformational dynamics of the thermostable proteins have been proposed (*22*) to be optimized for their function at high temperature so that part of the polypeptide backbone could form a stable scaffold to maintain the integrity of the active site at high temperature. The active site of the Cu_A protein is the dinuclear copper center anchored in the cupredoxin fold containing the loops connecting the sheets in the β barrel, and hence the dynamics of the metal active center in the $TtCu_A$ should be optimized for the function of the protein at elevated temperatures.

Activation Energy Barrier of the Conformational Transition. In order to determine the effect of the temperature on the conformational dynamics at the metal center of the protein, we studied the kinetics of the pH-induced conformational change at temperatures in the range 25 °C to 75 °C. The structure of the protein remains unaltered in this temperature range, and any temperature dependence of the rates would be determined by the temperature dependence of the conformational transition (eqs 3 and 4). The pH-induced conformational transition from the "low-pH" form to the "high-pH" form was found to follow single-exponential kinetics in the temperature range of the study. The apparent

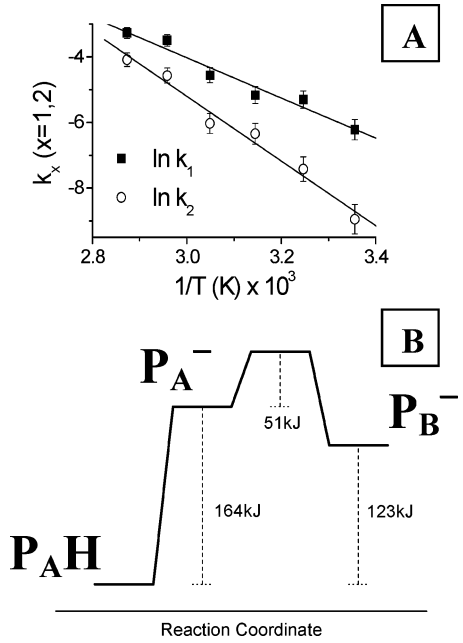

FIGURE 6: (A) Temperature dependence of conformational change of $TtCu_A$. Arrhenius plots for variation of rate constants: ■, k_1; ○, k_2. (B) Schematic diagram showing the relative energy levels of the "low-pH" and "high-pH" forms of $TtCu_A$.

rate constant (k_{app}) increased with increase in temperature (Figure 5A). Analysis of the pH dependence of k_{app} using eq 5 helped to determine the values of the K_a, k_1 and k_2 at different temperatures. Analogous to that observed for the temperature dependence of pK_a^{app}, the pK_a for the deprotonation equilibrium (step 1, eq 3) was also found to decrease with increase in temperature. Analysis of the temperature dependence of K_a using the van't Hoff equation (see Figure S2, Supporting Information) helped to determine the enthalpy change (ΔH_a =164 (±21) kJ/mol) and the entropy change (ΔS_a = 347 (±66) J/mol/K) associated with the deprotonation step of the reaction (step 1).

The activation parameters for the energy barrier of this conformational transition (step 2, eq 4) were determined from the temperature dependence of the k_1 and k_2 values using the Arrhenius equation. The values of k_1 as well as k_2 at different temperatures followed the Arrhenius equation over the temperature range of the study (Figure 6A). The activation energy (E_{a1}) for the forward reaction, i.e., the conversion of the "low-pH" form to the "high-pH" form, was found to be 51 (±5) kJ mol^{-1} whereas the activation energy for the reverse process (E_{a2}) was 92 (±6) kJ mol^{-1} (Figure 6A). The analogous studies on the reverse reaction, i.e., conversion of the "high-pH" form to the "low-pH" form (Scheme 2), were not carried out as the reaction was extremely slow at temperatures <45 °C (Figures 4C and 5B) while protein stability issues could become important at higher temperatures.

The relative energy level diagrams for the various states in the forward reaction of pH-induced conformational transition in the $TtCu_A$ derived from the temperature dependence of the pK_a^{app} and the rate constants (k_1 and k_2) are shown in Figure 6B. Duy et al. reported that the irreversible unfolding process of α-amylases from different sources shows linearity in the Arrhenius plots and activation energy barriers of unfolding were in the range of 260−360 kJ mol^{-1} (*14*). In the present case of pH-jump experiments of $TtCu_A$, the conformation change in the protein is mainly a distortion around the dinuclear copper center, which is expected to have a relatively smaller energy barrier in comparison to the more drastic changes involved in overall unfolding of the protein. The entropy of activation, determined from the intercept of the Arrhenius plots, was found to be positive in both k_1 (120 J/mol/K) and k_2 (200 J/mol/K) processes in step 2 of Scheme 1 in the present case. The thermodynamic stability parameter (ΔG_{stab}) of cold shock protein isolated from different sources like mesophiles, thermophiles and hyperthermophiles was found to increase from 11.3 kJ/mol to 26.2 kJ/mol when the optimal growth temperatures (T_{opt}) of the organisms increased from 52 °C to 90 °C respectively (*48*). The *Thermus thermophilus* bacterium shows an optimal growth at 65 °C to 72 °C and a maximal growth temperature of 85 °C (*49*). Our results indicate that the flexibility of the protein structure in the $TtCu_A$ indeed increases with temperature (up to 75 °C) as proposed earlier (*22*).

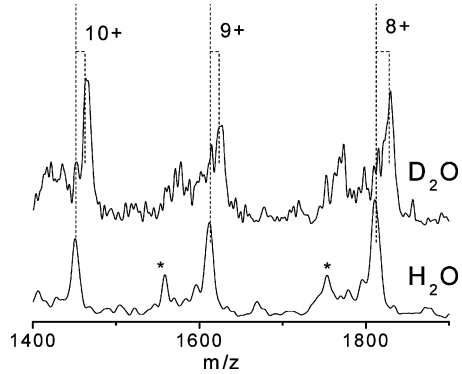

FIGURE 7: Electrospray ionization mass spectra of $TtCu_A$ in H_2O and after mixing with 50% D_2O in a continuous flow arrangement.

H/D Exchange ESI MS Observation of Fast Proton Transfer Equilibrium. The folding/unfolding of thermostable proteins has been shown to be often very slow, suggesting that the protein structure is highly rigid in these proteins (*12*, *14*, *16*). Rubredoxin from hyperthermophile *Pyrococcus furiosus* was shown to exhibit a slow global unfolding rate of 10^{-6} s^{-1} at 100 °C while the mesophilic analogue from *Clostridium pasteurianum* unfolds 10^2-10^3 times faster (*18*). On the other hand, Hernandez et al. (*17*) showed that the hyperthermophilic rubredoxin had a very fast amide proton exchange rate (in the millisecond time scale) even at 28 °C, suggesting that the local conformational fluctuations are possibly faster than the overall conformation change in the hyperthermophilic protein. The fast deprotonation/protonation equilibria (step 1, eq 3 and step 3, eq 6) in the present case, however, indicate that the rate constants for proton transfer in the *Thermus* protein can indeed be fast as earlier shown by H/D exchange studies on hyperthermophilic rubredoxin (*17*), though that may not correspond to any conformation change of the protein. In order to check whether the hydrogen exchange is indeed very fast in the $TtCu_A$, we carried out H/D exchange studies on the protein using ESI mass spectrometry. The native $TtCu_A$ in water (at ambient pH) shows 8+, 9+ and 10+ charge-states (Figure 7) corresponding to the dinuclear copper bound folded holoprotein with amino acids 38−168 (MW: 14482 ± 10 + 23 for a bound Na) of the subunit II from cytochrome c oxidase of *Thermus*

thermophilus (*32*). The charge state of the protein was interpreted by considering the crystal structure of the folded protein (*50*). The observed maximum positive charge state of the gaseous $TtCu_A$ protein was correlated quite well with the number of free surface exposed basic groups (*50*). The aqueous protein solution at ambient pH was mixed with 50% D_2O and immediately injected into the mass spectrometer in a continuous-flow setup. Figure 7 shows that all the three charge-state peaks are shifted toward larger *m*/*z* values on mixing of D_2O to the protein solution. The 8+ charge-state peak shifted by 13.75 (from 1814.25 to 1828), the 9+ charge-state peak shifted by 12.3 (from 1612.9 to 1625.2) and the 10+ charge-state peak shifted by 10.91 (from 1451.64 to 1462.55) on H/D exchange of the protein. The average number of protons exchanged on addition of D_2O was estimated to be 110, which is ~73% of the total number of protonable sites in the protein (131 amide +1 N-terminal, 4K, 5R, 4H, 6Y = 151 is the total number of protonable sites). These results thus support that the $TtCu_A$ can undergo fast protonation/deprotonation equilibrium on change in the pH of the solution.

One of the possible models that could rationalize the observation of slow conformational transition that follows the protonation/deprotonation of the protein is as follows: The conformation of the protein (secondary as well as tertiary structure) is stabilized by multitude of interactions including several hydrogen bonds between the residues. Any conformation change in the protein would thus require several hydrogen bonds to be opened at the same time. Although the rate of exchange of individual hydrogen bonds can be quite fast, the opening of the hydrogen bonds may not be coherent and thus the effective rate of simultaneous exchange of several hydrogen bonds associated with a particular segment of the protein would be very small. The complex nature of interactions in the stabilization of the structure of the thermostable proteins could thus result in fast exchange rates for individual hydrogens (exchangeable) in a protein while the conformational change remains effectively very slow as observed in the present case.

CONCLUSIONS

The dinuclear Cu_A center as a chromophore having characteristic visible transitions offers an opportunity to understand the local processes yielding conformational changes in the tertiary structure region of the metalloprotein. We have established the presence of two different conformers of the protein at the "low-pH" and the "high-pH" regime. The activation energy barrier for the conformational transition was found to be smaller in comparison to that expected for the unfolding of the thermostable protein. Our results indicated that the thermostable protein might show fast proton transfer kinetics but slow conformational dynamics. The observation of the kinetic inertness of the conformation of the $TtCu_A$ in the present case in spite of having fast proton transfer equilibrium is a direct elucidation of such a process. Based on these studies, we propose that, unfolding of protein being a special type of conformational change, the conformational inertness due to the existence of incoherence in the exchange dynamics in the protein exhibited by a thermostable protein could be the origin of the thermostability.

ACKNOWLEDGMENT

The authors thank Prof. B. Ludwig for kindly providing us the plasmid and Prof. G. Krishnamoorthy, Ms. Mamata Kombrabail, Mr. B. T. Kansara and Mr. Soumen K. Manna for help. Authors also thank Prof. S. V. Bhat, Indian Institute of Science, Bangalore, for help in the EPR experiment. Authors sincerely thank Prof. Brian Hoffman, Northwestern University, for important suggestions on analyses and interpretation of EPR results.

SUPPORTING INFORMATION AVAILABLE

The far-UV CD spectra of $TtCu_A$ at different pH; van't Hoff analysis of proton transfer equilibrium constants of $TtCu_A$; steady-state tryptophan fluorescence spectra of $TtCu_A$; and the lifetimes along with the amplitudes of the time-resolved tryptophan fluorescence decay of $TtCu_A$. This material is available free of charge via the Internet at http://pubs.acs.org.

REFERENCES

1. Jaenicke, R. (1991) Protein stability and molecular adaptation to extreme conditions, *Eur. J. Biochem. 202*, 715−728.
2. Jaenicke, R. (1996) Stability and folding of ultrastable proteins: eye lens crystallins and enzymes from thermophiles, *FASEB J. 10*, 84−92.
3. Robic, S., Guzman-Casado, M., Sanchez-Ruiz, J. M., and Marqusee, S. (2003) Role of residual structure in the unfolded state of a thermophilic protein, *Proc. Natl. Acad. Sci. U.S.A. 100*, 11345−11349.
4. Zhou, H. X. (2002) Toward the physical basis of thermophilic proteins: linking of enriched polar interactions and reduced heat capacity of unfolding, *Biophys. J. 83*, 3126−3133.
5. Jaenicke, R., and Bohm, G. (1998) The stability of proteins in extreme environments, *Curr. Opin. Struct. Biol. 8*, 738−748.
6. Szilagyi, A., and Zavodszky, P. (2000) Structural differences between mesophilic, moderately thermophilic and extremely thermophilic protein subunits: results of a comprehensive survey, *Structure 8*, 493−504.
7. Razvi, A., and Scholtz, J. M. (2006) Lessons in stability from thermophilic proteins, *Protein Sci. 15*, 1569−1578.
8. Sadeghi, M., Naderi-Manesh, H., Zarrabi, M., and Ranjbar, B. (2006) Effective factors in thermostability of thermophilic proteins, *Biophys. Chem. 119*, 256−270.
9. Mukaiyama, A., Takano, K., Haruki, M., Morikawa, M., and Kanaya, S. (2004) Kinetically robust monomeric protein from a hyperthermophile, *Biochemistry 43*, 13859−13866.
10. Kumar, S., Tsai, C. J., and Nussinov, R. (2000) Factors enhancing protein thermostability, *Protein Eng. 13*, 179−191.
11. Liang, H. K., Huang, C. M., Ko, M. T., and Hwang, J. K. (2005) Amino acid coupling patterns in thermophilic proteins, *Proteins 59*, 58−63.
12. Wittung-Stafshede, P. (2004) Slow unfolding explains high stability of thermostable ferredoxins: common mechanism governing thermostability?, *Biochim. Biophys. Acta 1700*, 1−4.
13. Jaswal, S. S., Truhlar, S. M., Dill, K. A., and Agard, D. A. (2005) Comprehensive analysis of protein folding activation thermodynamics reveals a universal behavior violated by kinetically stable proteases, *J. Mol. Biol. 347*, 355−366.
14. Duy, C., and Fitter, J. (2005) Thermostability of irreversible unfolding alpha-amylases analyzed by unfolding kinetics, *J. Biol. Chem. 280*, 37360−37365.
15. Griffin, S., Higgins, C. L., Soulimane, T., and Wittung-Stafshede, P. (2003) High thermal and chemical stability of Thermus thermophilus seven-iron ferredoxin. Linear clusters form at high pH on polypeptide unfolding, *Eur. J. Biochem. 270*, 4736−4743.
16. Dams, T., and Jaenicke, R. (1999) Stability and folding of dihydrofolate reductase from the hyperthermophilic bacterium Thermotoga maritima, *Biochemistry 38*, 9169−9178.
17. Hernandez, G., Jenney, F. E., Jr., Adams, M. W., and LeMaster, D. M. (2000) Millisecond time scale conformational flexibility in a hyperthermophile protein at ambient temperature, *Proc. Natl. Acad. Sci. U.S.A. 97*, 3166−3170.

18. Cavagnero, S., Zhou, Z. H., Adams, M. W., and Chan, S. I. (1998) Unfolding mechanism of rubredoxin from Pyrococcus furiosus, *Biochemistry 37*, 3377−3385.
19. Moczygemba, C., Guidry, J., Jones, K. L., Gomes, C. M., Teixeira, M., and Wittung-Stafshede, P. (2001) High stability of a ferredoxin from the hyperthermophilic archaeon A. ambivalens: involvement of electrostatic interactions and cofactors, *Protein Sci. 10*, 1539−1548.
20. Fitter, J., and Heberle, J. (2000) Structural equilibrium fluctuations in mesophilic and thermophilic alpha-amylase, *Biophys. J. 79*, 1629−1636.
21. Fitter, J., Herrmann, R., Dencher, N. A., Blume, A., and Hauss, T. (2001) Activity and stability of a thermostable alpha-amylase compared to its mesophilic homologue: mechanisms of thermal adaptation, *Biochemistry 40*, 10723−10731.
22. Jaenicke, R. (2000) Do ultrastable proteins from hyperthermophiles have high or low conformational rigidity?, *Proc. Natl. Acad. Sci. U.S.A. 97*, 2962−2964.
23. Ostermeier, C., Harrenga, A., Ermler, U., and Michel, H. (1997) Structure at 2.7 A resolution of the Paracoccus denitrificans two-subunit cytochrome c oxidase complexed with an antibody FV fragment, *Proc. Natl. Acad. Sci. U.S.A. 94*, 10547−53.
24. Iwata, S., Ostermeier, C., Ludwig, B., and Michel, H. (1995) Structure at 2.8 A resolution of cytochrome c oxidase from Paracoccus denitrificans, *Nature 376*, 660−669.
25. Saraste, M. (1990) Structural features of cytochrome oxidase, *Q. Rev. Biophys. 23*, 331−66.
26. Saraste, M. (1999) Oxidative phosphorylation at the fin de siecle, *Science 283*, 1488−1493.
27. Gupta, S., Warne, A., Saraste, M., and Mazumdar, S. (2001) pH-induced conformational transition in the soluble CuA domain of Paracoccus denitrificans cytochrome oxidase, *Biochemistry 40*, 6180−6189.
28. Hwang, H. J., and Lu, Y. (2004) pH-dependent transition between delocalized and trapped valence states of a CuA center and its possible role in proton-coupled electron transfer, *Proc. Natl. Acad. Sci. U.S.A. 101*, 12842−12847.
29. Farrar, J. A., Lappalainen, P., Zumft, W. G., Saraste, M., and Thomson, A. J. (1995) Spectroscopic and mutagenesis studies on the CuA centre from the cytochrome-c oxidase complex of Paracoccus denitrificans, *Eur. J. Biochem. 232*, 294−303.
30. Lappalainen, P., Aasa, R., Malmstrom, B. G., and Saraste, M. (1993) Soluble CuA-binding domain from the Paracoccus cytochrome c oxidase, *J. Biol. Chem. 268*, 26416−26421.
31. Wittung-Stafshede, P., Malmstrom, B. G., Sanders, D., Fee, J. A., Winkler, J. R., and Gray, H. B. (1998) Effect of redox state on the folding free energy of a thermostable electron-transfer metalloprotein: the CuA domain of cytochrome oxidase from Thermus thermophilus, *Biochemistry 37*, 3172−3177.
32. Slutter, C. E., Sanders, D., Wittung, P., Malmstrom, B. G., Aasa, R., Richards, J. H., Gray, H. B., and Fee, J. A. (1996) Water-soluble, recombinant CuA-domain of the cytochrome ba3 subunit II from Thermus thermophilus, *Biochemistry 35*, 3387−3395.
33. Sujak, A., Sanghamitra, N. J., Maneg, O., Ludwig, B., and Mazumdar, S. (2007) Thermostability of proteins: role of metal binding and pH on the stability of the dinuclear CuA site of Thermus thermophilus, *Biophys. J. 93*, 2845−2851.
34. Manna, S. K., and Mazumdar, S. (2006) Role of threonine 101 on the stability of the heme active site of cytochrome P450cam: multiwavelength circular dichroism studies, *Biochemistry 45*, 12715−12722.
35. Williams, P. A., Blackburn, N. J., Sanders, D., Bellamy, H., Stura, E. A., Fee, J. A., and McRee, D. E. (1999) The CuA domain of Thermus thermophilus ba3-type cytochrome c oxidase at 1.6 A resolution, *Nat. Struct. Mol. Biol. 6*, 509−516.
36. Wittung, P., Kallebring, B., and Malmstrom, B. G. (1994) The cupredoxin fold is found in the soluble CuA and CyoA domains of two terminal oxidases, *FEBS Lett. 349*, 286−288.
37. Gamelin, D. R., Randall, D. W., Hay, M. T., Houser, R. P., Mulder, T. C., Canters, G. W., de Vries, S., Tolman, W. B., Lu, Y., and Solomon, E. I. (1998) Spectroscopy of Mixed-Valence CuA-Type Centers: Ligand-Field Control of Ground-State Properties Related to Electron Transfer, *J. Am. Chem. Soc. 120*, 5246−5263.
38. Lu, Y., Gralla, E. B., Roe, J. A., and Valentine, J. S. (1992) The redesign of a type 2 into a type 1 copper protein: construction and characterization of yeast copper, zinc superoxide dismutase mutants, *J. Am. Chem. Soc. 114*, 3560−3562.
39. Çakir, S., Biçer, E., and Eleman, A. (2001) Synthesis, spectroscopic and voltammetric studies of mixed-ligand copper(II) complexes of amino acids, *Transition Met. Chem. 26*, 89−95.
40. Szabo, A. G., Stepanik, T. M., Wayner, D. M., and Young, N. M. (1983) Conformational heterogeneity of the copper binding site in azurin. A time-resolved fluorescence study, *Biophys. J. 41*, 233−244.
41. Das, T. K., and Mazumdar, S. (1995) pH-induced conformational perturbation in horseradish peroxidase. Picosecond tryptophan fluorescence studies on native and cyanide-modified enzymes, *Eur. J. Biochem.* 823−828.
42. Karpefors, M., Slutter, C. E., Fee, J. A., Aasa, R., Kallebring, B., Larsson, S., and Vanngard, T. (1996) Electron paramagnetic resonance studies of the soluble CuA protein from the cytochrome ba3 of Thermus thermophilus, *Biophys. J. 71*, 2823−2829.
43. Slutter, C. E., Gromov, I., Richards, J. H., Pecht, I., and Goldfarb, D. (1999) Mutations of the Weak Axial Ligand in the Thermus CuA Center Modulates Its Electronic Structure, *J. Am. Chem. Soc. 121*, 5077−5078.
44. Dennison, C., Vijgenboom, E., de Vries, S., van der Oost, J., and Canters, G. W. (1995) Introduction of a CuA site into the blue copper protein amicyanin from Thiobacillus versutus, *FEBS Lett. 365*, 92−94.
45. Wolff, N., Deniau, C., Letoffe, S., Simenel, C., Kumar, V., Stojiljkovic, I., Wandersman, C., Delepierre, M., and Lecroisey, A. (2002) Histidine pKa shifts and changes of tautomeric states induced by the binding of gallium-protoporphyrin IX in the hemophore HasASM, *Protein Sci. 11*, 757−765.
46. Martin, R. B. (1974) Pyrrole hydrogen ionization of imidazole derivatives in metal ion complexes and carbonic anhydrase, *Proc. Natl. Acad. Sci. U.S.A. 71*, 4346−4347.
47. Valentine, J. S., Sheridan, R. P., Allen, L. C., and Kahn, P. C. (1979) Coupling between Oxidation State and Hydrogen Bond Conformation in Heme Proteins, *Proc. Natl. Acad. Sci. U.S.A. 76*, 1009−1013.
48. Perl, D., Welker, C., Schindler, T., Schroder, K., Marahiel, M. A., Jaenicke, R., and Schmid, F. X. (1998) Conservation of rapid two-state folding in mesophilic, thermophilic and hyperthermophilic cold shock proteins, *5*, 229−235.
49. Oshima, T., and Imahori, K. (1974) Physiochemical properties of deoxyribonucleic acid from an extreme thermophile, *J. Biochem. (Tokyo) 75*, 179−183.
50. Prakash, H., and Mazumdar, S. (2005) Direct correlation of the crystal structure of proteins with the maximum positive and negative charge States of gaseous protein ions produced by electrospray ionization, *J. Am. Soc. Mass Spectrom. 16*, 1409−1421.

BI701783X